Springer

Journal of
Mechanical
Science and
Technology

Journal of Mechanical Science and Technology 22 (2008) 522~531

www.springerlink.com/content/1738-494x

Unavoidable geometric errors in the side walls of end-milled parts -cylindrical surface-

Kun Sang Lee and Kang Kim*

School of Mechanical and Automotive Engineering, Kookmin University, 861-1 Jungreung-dong, Sungbook-gu, Seoul 136-702, Korea

(Manuscript Received September 29, 2007; Revised December 26, 2007; Accepted December 26, 2007)

Abstract

The geometric characteristics of the side wall generated by the end-milling process are investigated through experiments and geometrical analyses. Both the inner and outer cylindrical surfaces are considered. Based on previous studies where the change of material removal per tooth was shown to affect the geometry of the end-milled side wall directly, it is expected that such material removal always varies just before the tool disengages the part in any case of cylindrical end-milling. The location and the size of a geometrically defected region in the cylindrical side wall are also presented. A model for predicting the depth in the radial direction is also developed. The proposed models thus make it possible to understand and anticipate the geometrical characteristics of end-milled cylindrical side walls in a quantitative manner.

Keywords: End-milling process; Geometric errors of side wall; Cylindrical surface; Cutting conditions; Material removal per tooth

1. Introduction

It is well known that the geometric features of milled surfaces are influenced by the independent variables in the machining system including the machine tool, workpiece, cutting tool and cutting conditions [1-7]. These independent variables are closely related to the cutting force and the tool deflection. It has been also shown that such variables affect the end-milled surface integrity [8-11]. The previous research results by Kim [12, 13] showed that geometrical surface error is caused by the surface generation mechanism of end milling itself. Specifically, it was demonstrated that the complete elimination of the error is impossible without any other finishing process, although the size of error can be reduced under the optimal cutting conditions.

For the case of a cylindrically end-milled surface, the location and range of the geometric error were studied [12]. Moreover, the location, range and depth of the unavoidable geometric error in the end-milled flat surface were revealed [13]. Therefore, in this paper, the depth of the unavoidable geometric error in the end-milled cylindrical surface is examined experimentally. Subsequently, an analytical model for predicting the depth of the unavoidable geometric error under given cutting conditions is proposed and validated by comparing with the experimental results in both a qualitative and quantitative manner.

2. Valley angle and valley depth

The typical roundness profiles of the cylindrical side walls on the end-milled male and female parts are shown in Fig. 1 (a) and (b), respectively. Each Fig. shows that there exists a defect zone where the surface is more deepened than the other neighboring surface. It is noted that the roundness of the surface which is deteriorated is named as 'valley' and is characterized with the help of 'valley angle (θ)' and 'valley depth (V_d)'. There is an intimate relationship between the change of material removal per tooth during the process and the valley.

*Corresponding author. Tel.: +82 2 910 4676, Fax.: +82 2 910 4839
E-mail address: kangkim@kookmin.ac.kr
DOI 10.1007/s12206-007-1213-4

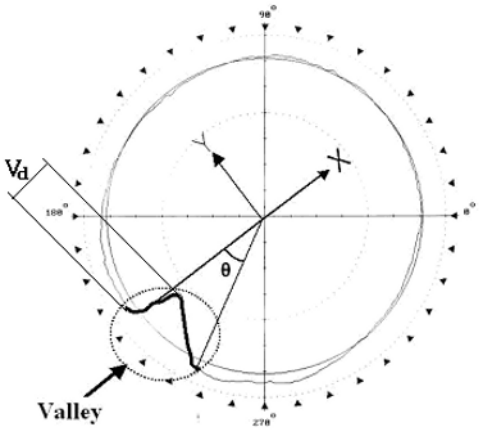

(a) Outer cylindrical surface milling

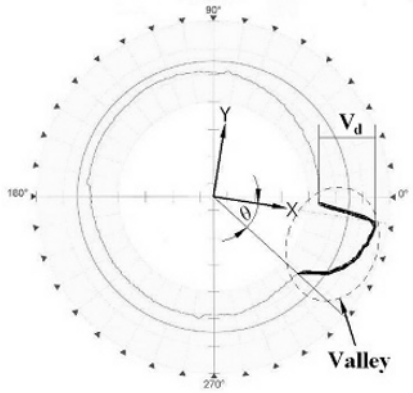

(b) Inner cylindrical surface milling

Fig. 1. Typical roundness profile of cylindrically end-milled surface.

Fig. 2 is a schematic illustration of the relative motion of the end-milling tool in the process. If the spindle speed, the feed rate and the apparent depth of cut are kept constant during the process, the material removal per tooth increases gradually from zero to a certain value, which is maintained for some duration, and then decreases gradually from this value to zero. For convenience, they are named 'entry region' (I in Fig. 2), 'steady cutting region' (II in Fig. 2) and 'exit region' (III in Fig. 2), respectively. Each region is defined as a location of the tool center and related to the tool approaching and retreating paths [12].

3. Experiment

Fig. 3 illustrates the shape and size of specimens, made from general purpose carbon steel, (SM45C). In order to retain the same diameter (40mm) for all the

Table 1. Roundness error before experiment (unit : ㎛).

	1	2	3	4	5	6	7	8	9	Average
Roundness	2.05	3.70	4.35	2.70	5.20	4.70	4.30	3.70	3.30	3.77

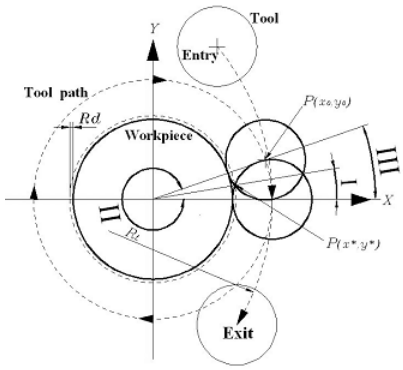

(a) Outer surface

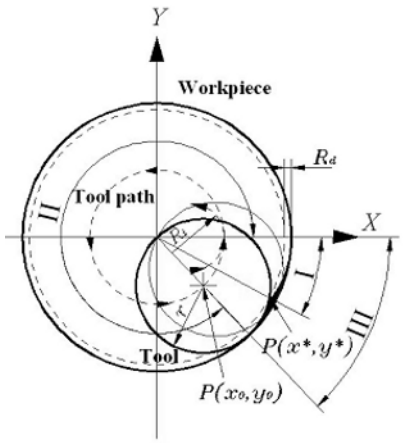

(b) Inner surface

Fig. 2. Entry region(I), Steady cutting region(II) and Exit region(Ⅲ).

specimens after the milling process, the dimension D_o for the outer surface experiment and D_i for the inner surface experiment in Fig. 3 have four and three different values, respectively. To minimize differences in the surface geometry and condition between the specimens, they were ground in the preparation stage. Nine specimens were sampled randomly and the roundness errors were measured. The roundness errors were between 2.05-5.20 μm as given in Table 1. It is expected that such roundness errors are much smaller than experimental results.

The CNC vertical milling machine used in the experiment was a Model TMV-40M. Prior to the experiment, the machine table movement errors were

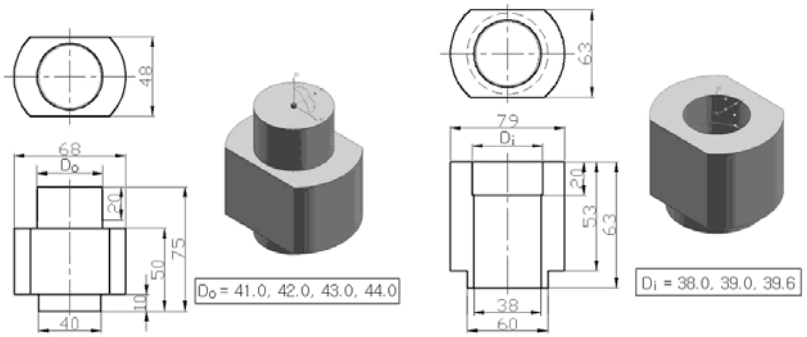

(a) Outer surface (b) Inner surface

Fig. 3. Specimen (No scale, unit : mm).

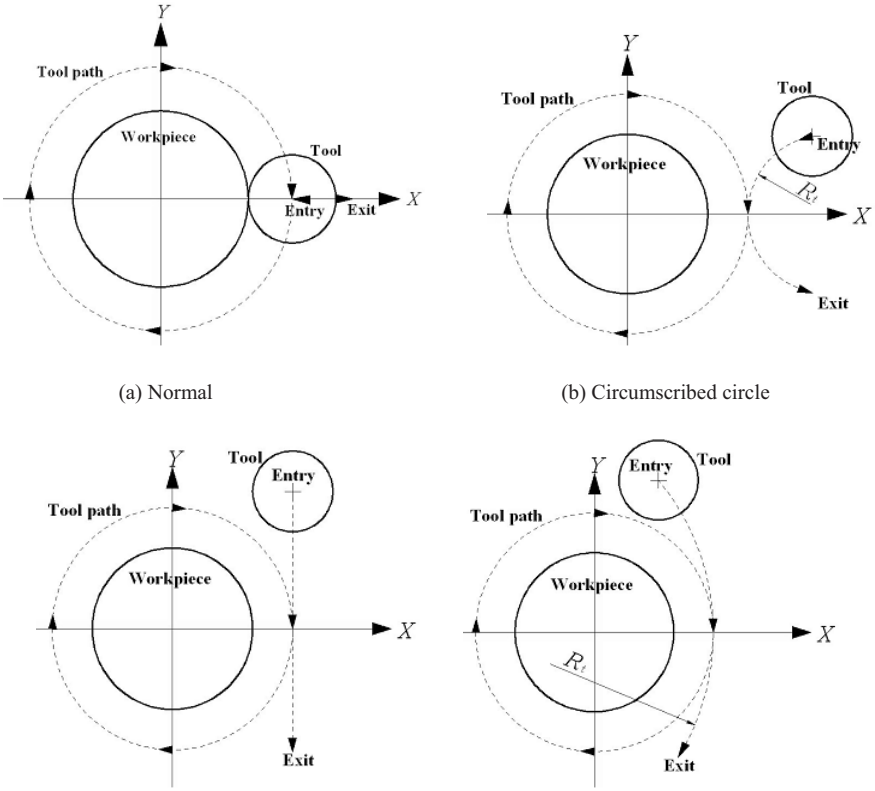

(a) Normal (b) Circumscribed circle

(c) Tangential (d) Inscribed circle

Fig. 4. Tool approaching path (Outer surface).

measured and calibrated by using the Model AVEC-100 Ballbar system. Through this calibration, the errors were kept to less than 0.5 μm. Titanium-coated standard 2 flutes high speed steel end-milling tools were used for the experiment. The diameter and the helix angle of tools are 20 mm and 30°, respectively. To avoid the effect of tool wear, which may affect the experiment, the tool was changed with a new one in every five experimental milling operations. The roundness profiles of the end-milled side walls were measured at the middle of side walls by Talyrond 252.

Table 2 shows the experimental cutting conditions. The spindle speed, the feed rate and the axial depth of cut were set constant to be 381 rev/min, 70 mm/min

Table 2. Experimental conditions.

Conditions		Value
Feed rate (mm/min)		70
Spindle speed (r.p.m.)		381
Axial depth of cut (A_d)(mm)		20
Tool revolution direction		Clockwise
Tool path		Down cut milling
Outer surface	Radial depth of cut (R_d)(mm)	0.5, 1.0, 1.5, 2.0
	Tool approaching path	N (normal), C (circumscribed), T (tangential), I (inscribed)
Inner surface	Radial depth of cut (R_d)(mm)	0.2, 0.5, 1.0
	Tool approaching path	N (normal), I (inscribed)

and 20 mm, respectively. For the outer surface milling, the radial depth of cut was varied from 0.5 mm to 2.0 mm at 0.5 mm intervals, and four different (normal, circumscribed, tangential and inscribed) tool approaching paths were applied (Fig. 4). For the inner surface milling, three different values (0.2, 0.5 and 1.0 mm) of the radial depth of cut were selected, and only the normal and inscribed tool approaching paths were applied because of the interference between the tool and the workpiece (Fig. 5).

4. Valley modeling

The previous study [13] revealed that the change of material removal per tooth leads to an error in the machined surface geometry due to machining elasticity. As can be expected from Fig. 2, the ultimate after-machined surface generated in the entry region and the steady cutting region has no geometrical error in

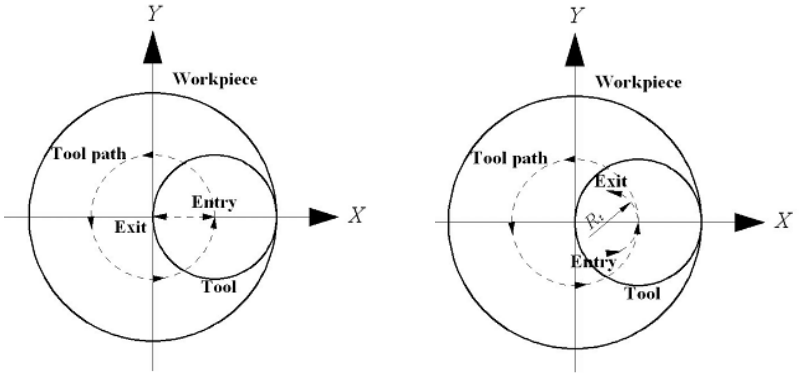

(a) Normal (b) Inscribed circle

Fig. 5. Tool approaching path (Inner surface).

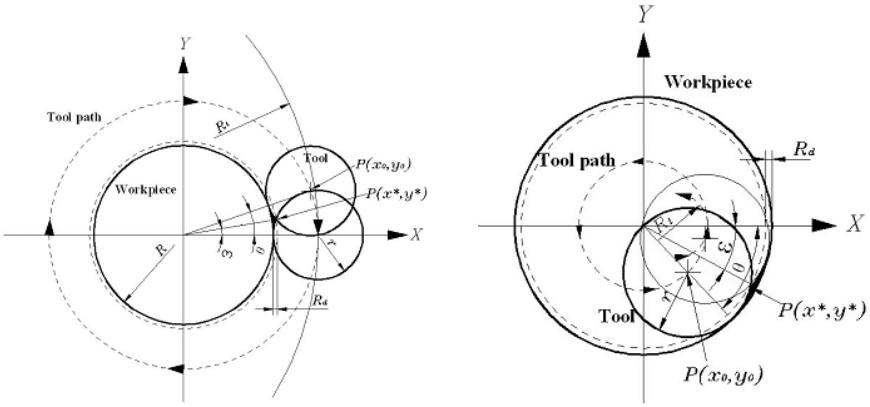

(a) Outer surface (b) Inner surface

Fig. 6. Coordinate system for valley angle analysis.

ideal cases. This is because the material removal per tooth is constant. In the exit region, however, the material removal per tooth is becoming smaller until it reaches zero value. Thus, it is presumed that the exit region corresponds to the valley. To characterize this valley, the valley angle and the valley depth are introduced. The valley angle and the change of the material removal per tooth, which is required to obtain the valley depth, have an analytic solution. The valley depth is assumed to be proportional to the change of the material removal per tooth. Through comparison between the experimental results and the model, the proportional factor can be found.

4.1 Valley angle

If the tool is suspended at the end of the entry region, a concave surface whose curvature is identical to the tool radius is generated on the workpiece surface. The bottom point of this concave surface is the first point of the ultimate after-machined surface. The half of this concave surface, which is in front of the tool along the tool path direction, is removed when the tool resumes its movement, while the other half of the concave has no change until the tool arrives at the point $P(x^*, y^*)$ in Fig. 6. It is assumed that $P(x_0, y_0)$ is the location of tool center at this instant. To complete the after-machined surface, the tool should continue its movement when it encounters the first point of the after-machined surface. During this movement, the radial depth of cut decreases from R_d to 0 gradually so that a valley is generated.

The coordinate system for valley angle analysis is shown in Fig. 6, where the X-axis coincides with the line connecting the workpiece center and the firstly generated point of the after-machined surface in the entry region, and the Y-axis is orthogonal to the X-axis with passing the workpiece center. As can be depicted from this figure, the valley angle, θ, is the one between the X-axis and the line connecting the workpiece center and the location of tool center when the tool reaches the point $P(x^*, y^*)$, $P(x_0, y_0)$. The values of x^* and y^*, which are needed to obtain θ, can be found from the intersection points of the following two circles:

$$\left(x^*\right)^2 + \left(y^*\right)^2 = \left(R + \upsilon\right)^2 \tag{1}$$

$$\left\{x^* - \left(R + \delta + \rho\right)\right\}^2 + \left(y^*\right)^2 = \left(\delta + \rho\right)^2 \tag{2}$$

$$\begin{cases} \delta = r, & \upsilon = R_d \\ \delta = -r, & \upsilon = -R_d \quad (\textit{inner surface}) \\ \rho = 0 & (\textit{tool approaching path: normal}) \\ \rho = R_t & (\textit{tool approaching path: circumscribed circle}) \\ \rho = \infty & (\textit{tool approaching path: tangential}) \\ \rho = -R_t & (\textit{tool approaching path: inscribed circle}) \end{cases}$$

where R is the after-machined workpiece radius; r is the tool radius; R_d is the radial depth of cut; R_t is the curvature of the tool approaching path; δ, ρ and υ are dummy variables.

The point $P(x^*, y^*)$ must satisfy equations (1) and (2), and be a point on the circle with center point, $P(x_0, y_0)$, and radius, r. The equation of this circle is

$$\left(x^* - x_0\right)^2 + \left(y^* - y_0\right)^2 = \delta^2 \tag{3}$$

and $P(x_0, y_0)$ is at a distance $R+\delta$ from the workpiece center; therefore,

$$\left(x_0\right)^2 + \left(y_0\right)^2 = \left(R + \delta\right)^2 \tag{4}$$

The valley angle, θ, can be expressed as follows:

$$\theta = \tan^{-1}\left(y_0 / x_0\right) \tag{5}$$

4.2 Material removal per tooth

Fig. 7 shows the coordinate system for material removal per tooth analysis where O_1, O_2 and O_3 are the centers of the tool approaching path, the workpiece and the tool, respectively. If the angular displacement of the tool center corresponding to the feed per tooth in the valley is θ_t, it is given by

$$\theta_t = \frac{F}{ZN \times \left(R + \delta\right)} \tag{6}$$

where F is the feed rate, N is the rotational speed of the tool and Z is the number of teeth on the tool periphery. The total number of the material removal by every cutting tooth in the valley, n, is

$$n = INT\left\{\theta / \theta_t\right\} \tag{7}$$

Such that when the i^{th} material removal occurs in the valley, the angular displacement of the tool center, ϕ_i, in Fig. 7 can be expressed as

$$\phi_i = \theta - \left(i \times \theta_t\right) \quad (i = 1, \cdots, n) \tag{8}$$

At this moment, the new surface is generated along the arc B_2B_3 as shown in Fig. 8. The area S_i corresponds to the amount of workpiece that would be removed right after the occurrence of the i^{th} material

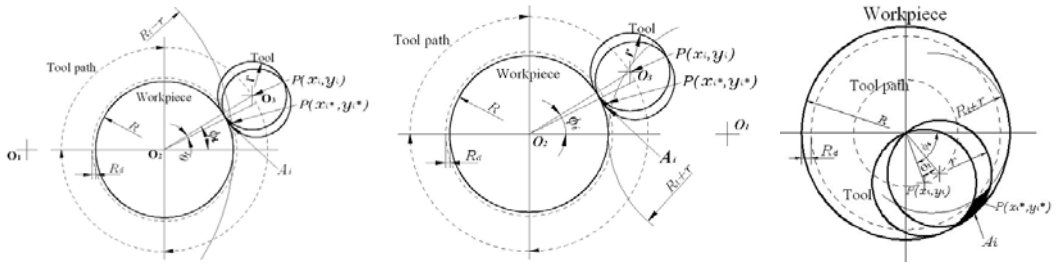

(a) Outer surface / Tool approaching path : Inscribed circle (b) Outer surface / Tool approaching path : Circumscribed circle (c) Inner surface / Tool approaching path : Inscribed circle

Fig. 7. Coordinate system for material removal per tooth analysis.

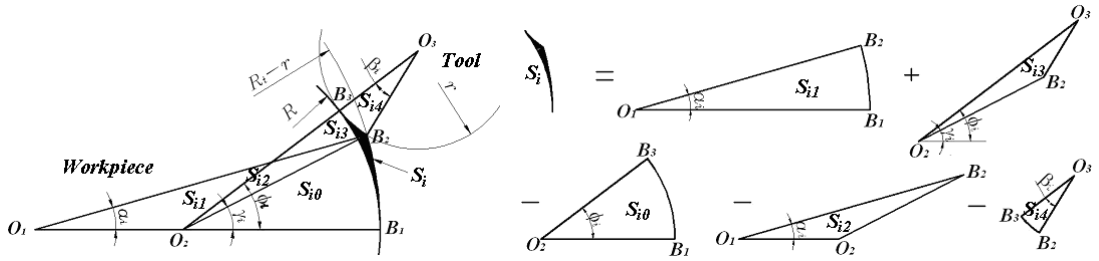

(a) Outer surface / Tool approaching path : Inscribed circle

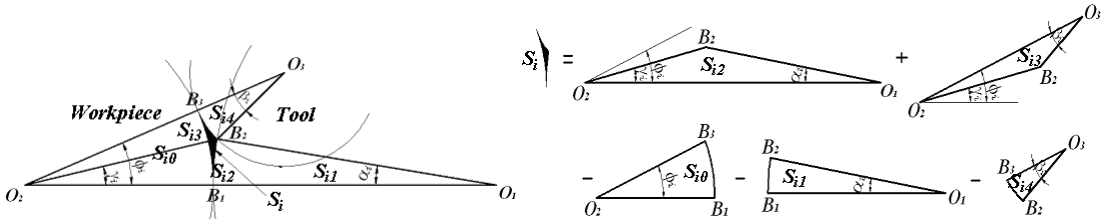

(b) Outer surface / Tool approaching path : Circumscribed circle

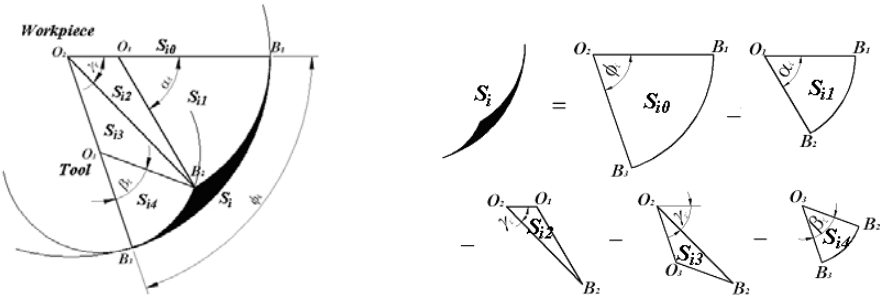

(c) Inner surface / Tool approaching path : Inscribed circle

Fig. 8. Material to be removed after the 1th removal in exit region.

removal. The arc B_1B_2 is identical to the surface generated at the end of the entry region. Hence B_1 and B_3 are on the line O_1O_2 and line O_2O_3, respectively. If B_2 is P (x_i^*, y_i^*), x_i^* and y_i^* must satisfy the following set of equations:

$$\left\{x_i^* - (R+\delta+\rho)\right\}^2 + \left(y_i^*\right)^2 = (\delta+\rho)^2 \quad (9)$$

$$\left\{x_i^* - (R+\delta)\cos\phi_i\right\}^2 + \left\{y_i^* - (R+\delta)\sin\phi_i\right\}^2 = \delta^2 \quad (10)$$

If x_i^* and y_i^* are found, the angles α_i ($\angle B_1O_1B_2$), γ_i

($\angle B_1O_2B_3 = \angle B_1O_2O_3$) and β_i ($\angle B_2O_3B_3$) can be also written as

$$\alpha_i = \tan^{-1}\left\{\frac{y_i^*}{\left|x_i^* - (R+\delta+\rho)\right|}\right\} \tag{11}$$

$$\gamma_i = \tan^{-1}\left\{\frac{y_i^*}{x_i^*}\right\} \tag{12}$$

$$\beta_i = \sin^{-1}\left[\frac{\sin(\phi_i - \gamma_i)\times\left\{\left(x_i^*\right)^2 + \left(y_i^*\right)^2\right\}^{\frac{1}{2}}}{|\delta|}\right] \tag{13}$$

To obtain S_i, it is decomposed into five elements: S_{i0} (area of sector $B_1O_2B_3$), S_{i1} (area of sector $B_1O_1B_2$), S_{i2} (area of triangle $O_1O_2B_2$), S_{i3} (area of triangle $O_2O_3B_2$) and S_{i4} (area of sector $B_2O_3B_3$), to be written as

$$S_{i0} = \frac{1}{2}R^2\phi_i \tag{14}$$

$$S_{i1} = \frac{1}{2}(\delta+\rho)^2 \times \alpha_i \tag{15}$$

$$S_{i2} = \frac{1}{2}|R+\delta+\rho| \times y_i^* \tag{16}$$

$$S_{i3} = \frac{1}{2}(R+\rho)\left\{\left(x_i^*\right)^2 + \left(y_i^*\right)^2\right\}^{\frac{1}{2}} \sin(\phi_i - \gamma_i) \tag{17}$$

$$S_{i4} = \frac{1}{2}\delta^2\beta_i \tag{18}$$

As shown in Fig. 8, the equations expressing S_i are different not only from the cases of inner and outer surface milling, but also from the ways of tool approaching path. Four different tool approaching paths (normal, tangential, circumscribed circle, inscribed circle) are employed. But, 'normal' and 'tangential' can be treated as 'inscribed circle with R_t (curvature of the tool approaching path) =0' and 'circumscribed circle with $R_t = \infty$', respectively. The number of equations expressing S_i can then be reduced to three for all cases considered in this study.

$$S_i = S_{i0} - (S_{i1} + S_{i2} + S_{i3} + S_{i4})$$
(inner surface) (19)

$$S_i = S_{i2} + S_{i3} - (S_{i0} + S_{i1} + S_{i4})$$
(outer surface, circumscribed circle) (20)

$$S_i = S_{i1} + S_{i3} - (S_{i0} + S_{i2} + S_{i4})$$
(outer surface, inscribed circle) (21)

In consequence, the material removal per tooth at the i^{th} occurrence in the valley can be expressed

$$A_i = S_{i-1} - S_i \qquad (i = 1, \cdots, n) \tag{22}$$

And the initial value of the material removal per tooth, A_0, is equal to the material removal per tooth in the steady cutting region. It can readily be obtained as a function of θ_t and the radial depth of cut in this region such that

$$A_0 = \frac{1}{2}\left|R^2 \times \left(R + R_d\right)^2\right| \times \theta_t \tag{23}$$

4.3 Valley depth

The apparent depth of cut is usually greater than the true depth of cut. If the difference between the two depths is larger, the defect zone depth appears to be deeper. This has been known as 'machining elasticity'. For the application of the machining elasticity concept, a coefficient of machining elasticity, K, is defined by the ratio of true depth of cut to material removal per tooth as

$$K = \frac{T_0}{A_0} = \frac{T_i}{A_i} \tag{24}$$

where T_0 is the initial value of the true depth of cut equal to the true depth of cut in the steady cutting region, and T_i is the true depth of cut at the i^{th} occurrence in the valley.

The distance between the workpiece center and the surface in the steady cutting region, $R+R_d$, is lessened to $R+R_d-T_0$ after being machined. If the material at P (x_i^*, y_i^*) in Fig. 7 is removed at the i^{th} contact between the cutting tooth and the workpiece in the valley, the distance from the workpiece center to this surface is changed from $\left\{\left(x_i^*\right)^2 + \left(y_i^*\right)^2\right\}^{\frac{1}{2}}$ to $\left\{\left(x_i^*\right)^2 + \left(y_i^*\right)^2\right\}^{\frac{1}{2}} - T_i$. The valley depth at the i^{th} occurrence in the valley, $(V_d)_i$, is then given by

$$(V_d)_i = \left|(R + R_d - T_0) - \left[\left\{\left(x_i^*\right)^2 + \left(y_i^*\right)^2\right\}^{\frac{1}{2}} - T_i\right]\right|$$
$$= \left|\left[(R + R_d) - \left\{\left(x_i^*\right)^2 + \left(y_i^*\right)^2\right\}^{\frac{1}{2}}\right] - K(A_0 - A_i)\right| \tag{25}$$

The numerical value of K can be found by comparison between the simulation results by using this valley model and those of the experiment.

5. Results and discussions

To complete the modeling of the valley depth, the

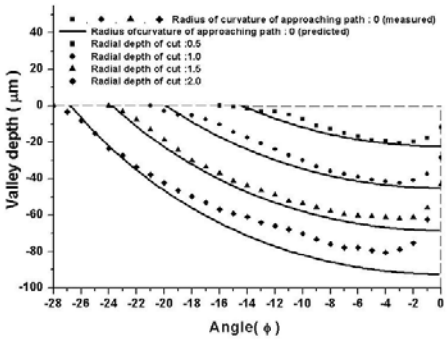

(a) Outer surface / Tool approaching path : Normal

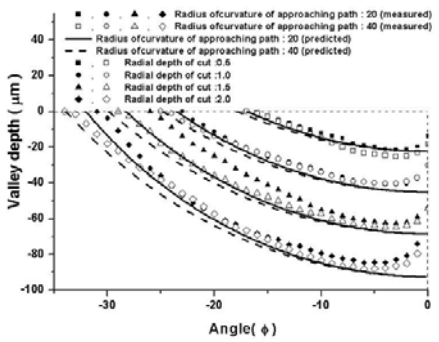

(b) Outer surface/Tool approaching path:Circumscribed circle

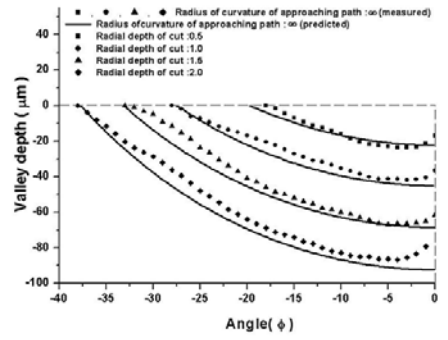

(c) Outer surface/Tool approaching path : Tangential

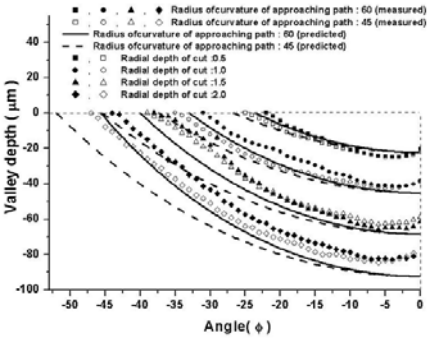

(d) Outer surface/Tool approaching path : Inscribed circle

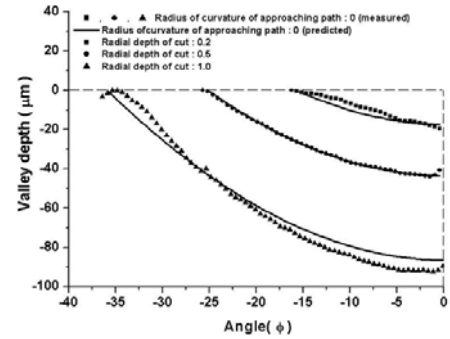

(e) Inner surface / Tool approaching path : Normal

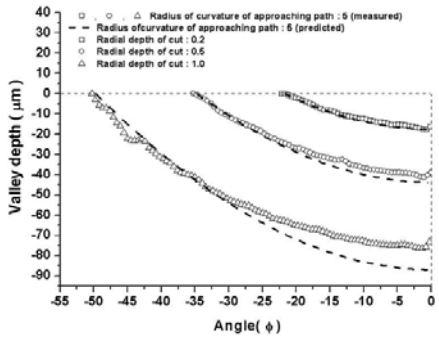

(f) Inner surface / Tool approaching path : Inscribed circle

Fig. 9. Valley profile.

coefficient of machining elasticity, K, in equation (24) is to be evaluated. So, numerical simulations were performed under the different values of K. The predicted profiles based on the simulation results were compared with the measured profile of the experimented workpiece. It is concluded that the least square error between the measured and predicted profiles is minimized when K is 713, which is presumed to be the most appropriate value of machining elasticity for this study.

Fig. 9 shows the measured valley profiles of the experimented specimens and the predicted valley profiles from the simulation results. The vertical line of angle=0 is the straight line passing through the workpiece center and the first generated after-machined surface point, whereas the horizontal line of valley depth=0 corresponds to the after-machined surface except the valley. To aid in understanding the milled-surface geometry, the valley angle and the valley depths are shown as negative (-) values in this figure. The angle of the crossing point, where the valley profile intersects the horizontal line of valley

depth=0, refers to the valley angle.

The predicted valley profiles provide the same tendency as the measured profiles. This verifies the correctness of the models developed in this study. All profiles describe that an increase in the radial depth of cut renders the valley wider and deeper if the cutting conditions except the radial depth of cut remain unchanged. Even though the radial depth of cut is kept constant for all tool approaching paths, the valley angle varies depending on the way of the initial tool approaching. This is because the angular displacement corresponding to the portion of the workpiece, already removed when the tool initially approaches the workpiece, is changed. When the tool approaching path is normal, such angular displacement has a minimum value. The following is the arrangement of the angular displacements of the tool approaching paths in the order of their size:

Normal < Circumscribed Circle < Tangential < Inscribed Circle

The valley angles, which can be estimated from the profiles in Fig. 9, yield exactly the same tendency. Even if the way of the tool approaching is changed, there are no variations in the maximum depth of the portion of the workpiece removed when the tool initially approaches the workpiece. From the above behavior, it can be presumed that the maximum valley depth is free from any changes, no matter what the tool approaching path is. Fig. 9 further shows the characteristics similar to this presumption.

As a result, it is found that the radial depth of cut and the tool approaching path have intimate relations with the generation of the valley. The valley angle is affected both by the radial depth of cut and the tool approaching path. On the other hand, the maximum valley depth is affected only by the radial depth of cut.

In Fig. 9, the difference between the measured and the predicted valley profiles near the vertical line of angle=0 is shown to be relatively larger than that of the other surface points. It is understood that this simulation error arises from the assumption made in machining elasticity concept and negligence of the interference phenomenon.

6. Conclusions

In the cylindrical end-milling process, the last generated surface point of the workpiece is identical to the first generated surface point. Because the tool radius is not zero, a portion of the workpiece that would be removed at the final stage of the process is already removed when the tool initially approaches the workpiece. The true material removal rate per tooth must then be changed from a certain value to zero gradually, just before the tool leaves the workpiece. This is directly related to unwanted generation of the geometrically defected surface, which is termed "valley." In addition, the valley angle and the valley depth models are developed based on geometrical analysis and machining elasticity. The valley angle is affected by the radial depth of cut and the tool approaching path. The maximum valley depth is affected only by the radial depth of cut. Even if the size of the valley becomes smaller under the careful selection of cutting conditions, it cannot be eliminated or avoided because of the cylindrical movement of the tool itself.

Acknowledgments

This work was supported by research program 2005 of Kookmin University in Korea.

References

[1] E. Budak and Y. Altintas, Peripheral milling conditions for improved dimensional accuracy, *Int. J. Mach. Tools Manu.* 34 (7) (1994) 907-918.

[2] J. G. Choi and M. Y. Yang, In-process prediction of the surface error using an identification of cutting depths in end milling operation by simulating surface, *J. of KSPE* 15 (2) (1998) 114-123.

[3] S. L. Ko, S. K. Lee and S. M. Bae, Study on the design of end mill geometry, *J. of KSPE*, 18 (8) (2001) 24-30.

[4] S. K. Lee and S. L. Ko, Analysis on the precision machining in end milling operation by simulating surface generation, *J. of KSPE* 16 (4) (1999) 229-236.

[5] S. H. Ryu, D. K. Choi and C. N. Chu, Optimal cutting condition in side wall milling considering form accuracy, *J. of KSPE* 20 (10) (2003) 31-39.

[6] J. Tlusty, S. Smith and C. Zamudia, New NC routines for quality in milling, *Annals of CIRP* 39 (1) (1990) 517-521.

[7] J. H. Yoon, M. S. Cheong and H. C. Lee, A study on transition of dimension error and surface precision in high speed machining of Al-alloy, *J. of KSMTE* 9 (3) (2003) 96-102.

[8] H. D. Cho and M. Y. Yang, A study on the predic-

tion of tool deflection and precision machining in ball end milling process, *KSME Journal* 16 (9) (1992) 1669-1680.

[9] Y. H. Kim and S. L. Ko, Improvement of the accuracy in cornering cut using end mill, *KSME Journal A* (3) (2001) 399-407.

[10] T. I. Seo and M. W. Cho, Tool trajectory generation based on tool deflection effects in flat-end milling process (I)-tool path compensation strategy, *KSME International Journal* 13 (10) (1999) 738-751.

[11] T. I. Seo and M. W. Cho, Tool trajectory generation based on tool deflection effects in flat-end milling process (II)-prediction and compensation of milled surface errors, *KSME International Journal* 13 (12) (1999) 918-930.

[12] K. Kim, Effect of tool approaching path on the shape of cylindrically milled parts, *Trans. of KSMTE* 12 (3) (2003) 45-51.

[13] K. Kim, Unavoidable geometric errors in the side walls of end-milled parts -flat surface, *J. of Mech. Science and Tech.* 21 (1) (2007) 48-56.